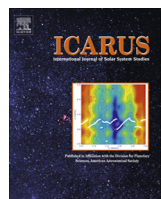




ELSEVIER

Contents lists available at ScienceDirect

Icarus

journal homepage: www.elsevier.com/locate/icarus

Illumination conditions at the lunar south pole using high resolution Digital Terrain Models from LOLA

P. Gläser ^{a,*}, F. Scholten ^b, D. De Rosa ^c, R. Marco Figuera ^a, J. Oberst ^b, E. Mazarico ^e, G.A. Neumann ^e, M.S. Robinson ^d

^a Technical University Berlin, Department of Geodesy and Geoinformation Science, Str. des 17. Juni 135, 10623 Berlin, Germany

^b German Aerospace Center, Institute of Planetary Research, Rutherfordstrasse 2, 12489 Berlin, Germany

^c European Space Agency, ESTEC, Keplerlaan 1, 2200 AG Noordwijk ZH, The Netherlands

^d Arizona State University, School of Earth and Space Exploration, Tempe, AZ 85287, USA

^e NASA Goddard Space Flight Center, Code 698, Greenbelt, MD 20771, USA

ARTICLE INFO

Article history:

Received 14 February 2014

Revised 25 July 2014

Accepted 8 August 2014

Available online 20 August 2014

Keyword:

Moon, surface

ABSTRACT

The illumination conditions of the lunar south pole are investigated using a geometrically adjusted, 20 m/pixel Digital Terrain Model (DTM) from laser tracks of the Lunar Orbiter Laser Altimeter (LOLA). Several comparisons with Narrow Angle Camera (NAC) images have been made to cross-validate the results. Illumination conditions were first evaluated over a region of 20 × 20 km over a one-year period (October 22, 2018 – October 22, 2019) at surface level and 2 m above ground. Three potential landing sites are investigated in more detail. A 19-year study covering the lunar precessional cycle was carried out at surface level, 2 and 10 m above ground for a site found at “Connecting Ridge”, the ridge connecting the Shackleton and de Gerlache crater. This area was found to be an ideal site for future landing missions with respect to illumination conditions. We identified locations receiving sunlight for 92.27% of the time at 2 m above ground and 95.65% of the time at 10 m above ground. At these locations the longest continuous periods in darkness are typically only 3–5 days.

© 2014 Elsevier Inc. All rights reserved.

1. Introduction

Illumination conditions in the Moon's polar areas are extreme. Owing to the small $\pm 1.54^\circ$ inclination of the Moon's rotational axis with respect to the ecliptic, areas experiencing permanent shadow or extended periods of sunlight exist. While areas in permanent shadow may harbor water ice (Watson et al., 1961), areas receiving nearly constant solar illumination enable almost uninterrupted solar power supply. Investigations of illumination conditions at the lunar poles have been of interest ever since. An obvious approach to investigate polar illumination conditions is to study the distribution of areas in sunlight or darkness using orbital images taken at different times. In 1994 the Clementine mission (Shoemaker et al., 1994) acquired dozens of images of the lunar poles but due to the short mission life of 71 days (Bussey et al., 1999) the investigation of illumination conditions was limited to ~2.5 lunar days during northern summer. Speyerer and Robinson (2013) used ~7800 Lunar Reconnaissance Orbiter Camera (LROC) Wide Angle Camera (WAC) images to investigate lunar illumination

conditions for a period from 15 February, 2010 to 5 February, 2011. Binary illumination maps were created from these images and resulted in a 100 m/pixel average illumination map for a 1° area around each pole. The lunar precessional cycle, however, is 18.6 years and the whole period needs to be observed to obtain definitive results, which cannot be achieved with image data yet. Stacy et al. (1997) used polarization properties of the reflected Arecibo radar signal of the lunar poles to search for water ice in permanently shadowed areas. However, the extreme viewing geometry (85.9° incidence angle for the lunar north pole; 83.9° for the south pole) resulted in extensive radar shadows due to surface relief, and only small portions of the far side could be observed.

A more direct approach was carried out by Margot et al. (1999). They used Earth based radar observations to derive polar Digital Terrain Models (DTMs) with 150 m spatial and 50 m height resolution. On the basis of DTMs, illumination conditions become a purely geometric exercise and can be simulated over any time span of interest. Nevertheless, the radar derived DTMs suffer from the same drawbacks as the radar images: only small portions of the far side could be observed, and radar shadows resulted in large data gaps within the DTM. The first complete direct measurement of the lunar polar topography was acquired by the Japanese Kaguya

* Corresponding author.

E-mail address: philipp.glaeser@tu-berlin.de (P. Gläser).

(SELENE) spacecraft. Noda et al. (2008) simulated the illumination conditions for both poles, using Laser Altimeter (LALT) derived DTMs with a resolution of 470 m, over a period of 2000 days and over one whole lunar precession cycle for certain areas. Similar simulations were run by Bussey et al. (2010) using a slightly newer version of the aforementioned LALT DTM but at the same resolution. They cross-validated their results to Clementine images and generated an average illumination map of the lunar south pole for the year 2020. However, owing to rough topography in the area, illumination conditions may differ substantially at shorter spatial scales. For studies of illumination at specific landing areas, higher-resolution DTMs are required. The Lunar Orbiter Laser Altimeter (LOLA) on-board the Lunar Reconnaissance Orbiter (LRO) is ideally suited for this study, owing to its high data resolution and geodetic control (Smith et al., 2010a; Chin et al., 2007). Mazarico et al. (2011) simulated polar illumination conditions using LOLA DTMs, with a resolution of 240 m. De Rosa et al. (2012) used LOLA DTMs with a resolution of up to 40 m to simulate illumination conditions for specific sites at the lunar south pole, that are known to be almost permanently illuminated and for this reason were envisioned as landing sites for the ESA Lunar Lander mission (Carpenter et al., 2012).

In this work, we concentrate on a more detailed investigation of the illumination conditions of three potential landing sites, two near Shackleton Rim (SR1 and SR2) and one on “Connecting Ridge” (CR1), by using high-resolution LOLA DTMs of 20 m resolution (nomenclature of landing sites was adopted from De Rosa et al. (2012)). We also compare our results to images from the LROC Narrow-Angle Camera (NAC) on-board LRO (Robinson et al., 2010).

2. Data

We used LOLA tracks to derive a 400×400 km DTM of the lunar south pole. LOLA is a 5-beam laser altimeter operating at 28 Hz pulse repetition rate. As seen from the nominal orbit altitude of 50 km the resolution in along- and cross-track direction is $\sim 10\text{--}12$ m (Smith et al., 2010b). The area of interest for this work covers Shackleton Rim and “Connecting Ridge” (the ridge connecting the Shackleton and the de Gerlache crater), two terrain features less than 20 km from the lunar south pole (Fig. 1a). In total 15,143 tracks (up to April 2013 – Neumann (2009)) are available in the area (-81° to -90°) and are incorporated in the DTM (Fig. 1b). All LOLA tracks converge at the poles due to LRO's polar orbit

and therefore the highest shot density is found here. In $\sim 77.3\%$ of the 20 m pixels in Fig. 1a between 1 to 18 LOLA shots can be found and only $\sim 22.7\%$ of the pixels are interpolated. Data density, however, drops with increasing distance from the pole. On average, in a 160×160 km DTM with 20 m/pixel resolution, about 50% of the pixels contain at least one LOLA shot and 50% are interpolated. The 400×400 km south polar DTM in Fig. 1b only contains 21.5% pixels occupied by at least one LOLA shot and 78.5% are interpolated. The derivation of adjusted DTM as displayed in Fig. 1a and b are described in 2.1.

2.1. Data adjustment

The individual tracks of the laser-derived DTM were subjected to a sophisticated adjustment scheme. At the high spatial resolution we consider, the individual tracks suffer from small but significant relative offsets (Gläser et al., 2013a; Gläser et al., 2013b). The adjustment is made by co-registering the individual laser tracks to a reference DTM which was produced from LROC NAC stereo images.

As a starting point the reference stereo DTM was derived. The NAC DTM covers an area near CR1 of about 2×2 km with a pixel resolution of 2 m (Fig. 2). The DTM suffers from gaps, especially in craters, where no image information are available due to shadowing. First, all LOLA tracks intersecting the area of the NAC DTM are selected (Fig. 3a). Relative offsets between the tracks and individual shot outliers become readily visible (Fig. 3b). Data gaps in the NAC DTM are effectively filled by LOLA, as the instrument's active laser operates independently of lighting conditions.

In total 876 tracks, containing $\sim 100,000$ spots, intersected the NAC DTM (using data as of August 2013). The co-registration algorithm estimates the correct position of LOLA tracks on the NAC DTM and also gives accuracy values for each fit. The resulting DTM after the co-registration is shown in Fig. 4a.

The accuracy values, standard deviations of the fit between the data sets in x , y , z -direction, can help detect outliers or erroneous tracks. Other parameters like the minimum amount of matched spots, maximum single height offset of a LOLA spot to the NAC DTM or the standard deviation of height residuals over the whole LOLA track compared to the NAC DTM are also used as filter settings. Hence, a filtering of the co-registered data set is feasible which leads to the final, filtered and co-registered LOLA DTM (Fig. 4b).

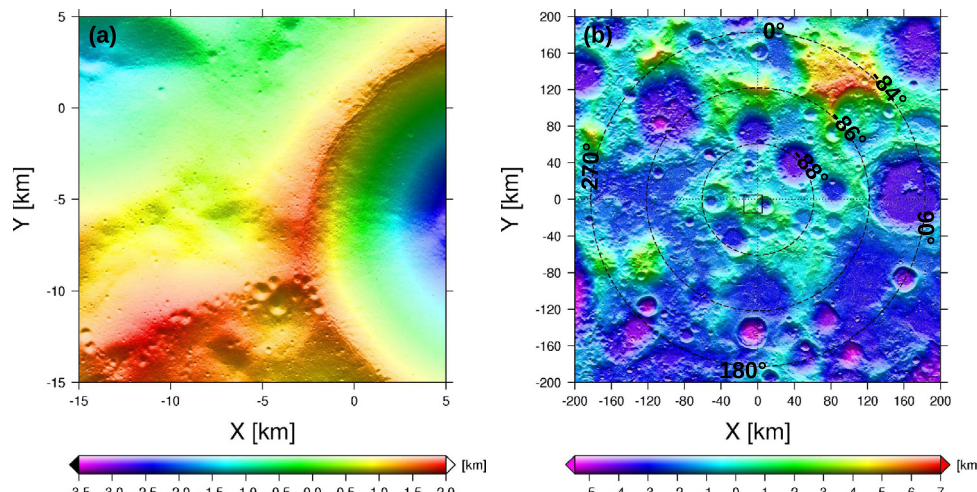


Fig. 1. (a) Adjusted, shaded, height color coded LOLA DTM of the region of interest at the lunar south pole. (b) Adjusted, shaded, height color coded 400×400 km LOLA DTM of the lunar south pole. The area of interest in this work, compare to left figure, is marked by a black square. (For interpretation of the references to color in this figure legend, the reader is referred to the web version of this article.)

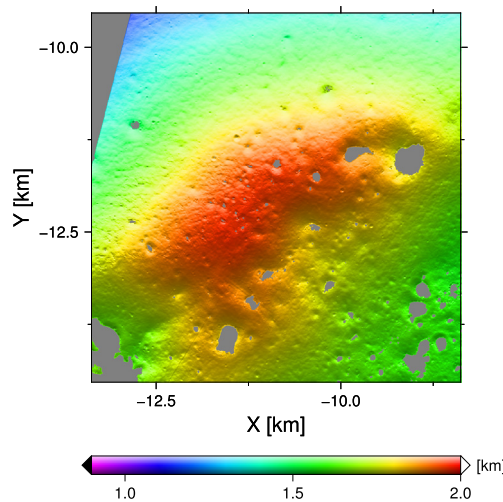


Fig. 2. A 2×2 km NAC DTM at the Connecting Ridge with a 2 m per pixel resolution is shown. The data gaps are due to shadowed regions, mostly crater floors, where the derivation of spatial data is impossible with stereo techniques.

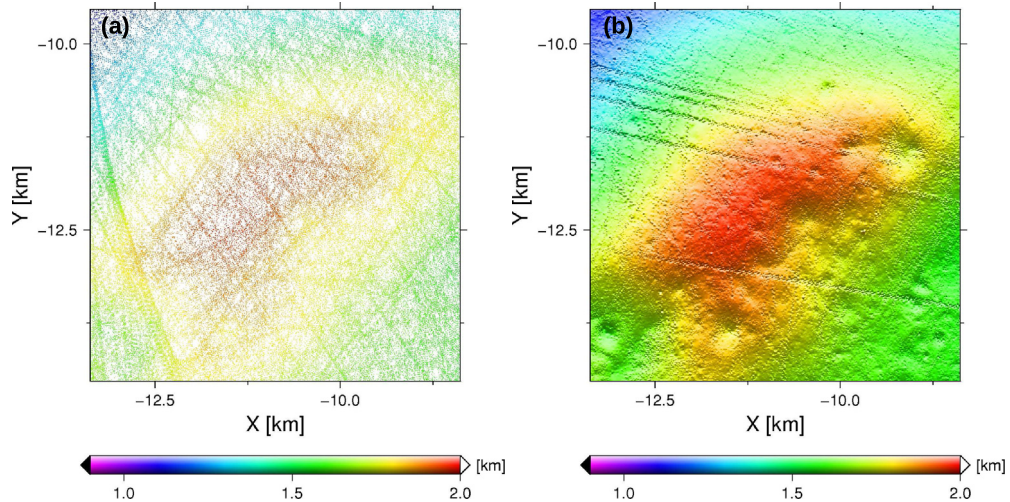


Fig. 3. All LOLA tracks intersecting the area covered by the NAC DTM are displayed (a). A DTM (5 m per pixel) created out of this LOLA data set is shown. The displacements between the LOLA tracks and speckle introduced by single offset spots are clearly visible (b).

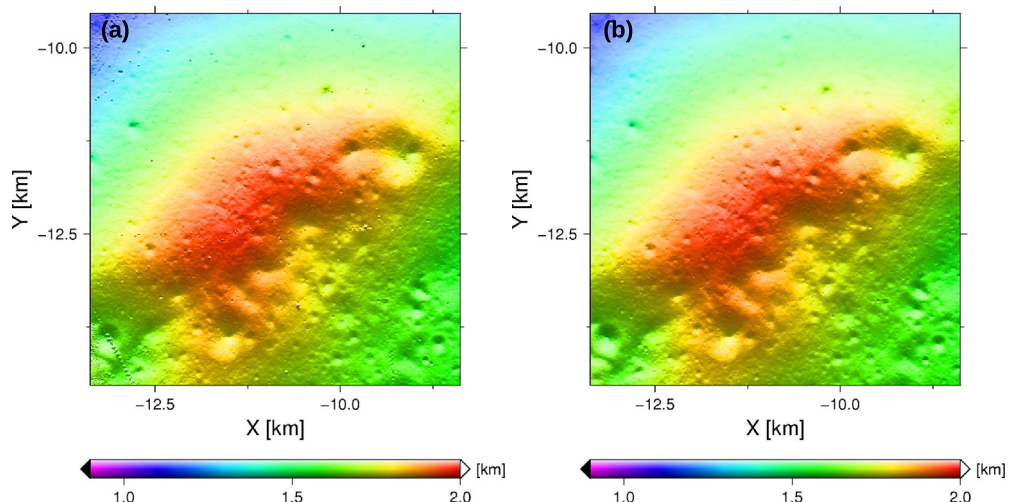


Fig. 4. A DTM with 5 m pixel resolution, created from co-registered LOLA tracks is displayed (a). After filtering, the final LOLA DTM (5 m per pixel) shows no more erroneous tracks or speckle (b).

In total 454 tracks, including $\sim 90,000$ individual laser spots, were co-registered and subjected to the filtering. Although only 50% of the actual LOLA tracks, 454 out of 876 tracks, make up the final DTM, the percentage of final LOLA spots amounts to 90% of the original spots. The 50% loss in LOLA tracks (but only 10% in real data) can partly be explained by the proximity to the lunar south pole, where all LOLA tracks converge due to LRO's polar orbit. Consequently, some tracks may only intersect the NAC DTM at the corners where too few spots can be used for co-registering. In addition, only two out of the five LOLA spots can be recorded over the entire night side, referred to as 'LOLA anomaly'. The effect is most likely caused by the contraction of a Multilayer Insulation (MLI) blanket, which pulls three of the five LOLA spots out of the receiver's focus (Smith et al., 2010b; Chakraborty, 2011). This results in many sparse data tracks near the poles some of which are also discarded from the analysis.

An adjusted LOLA DTM covering the same area as the NAC DTM is now available. While co-registration of LOLA tracks was carried out within the limited extent of the NAC DTM (Fig. 3), the tracks reach much beyond the DTM area, and we consider an area about nine times larger than the NAC DTM (Fig. 5a). The size of the new

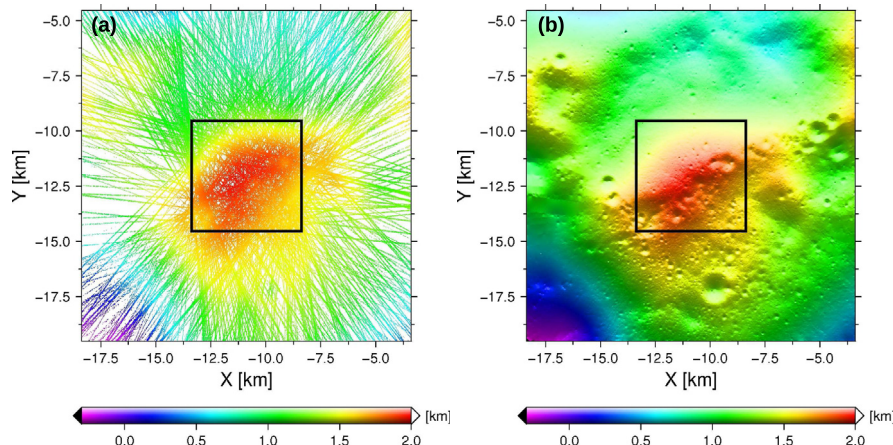


Fig. 5. All LOLA tracks covering nine times the area of the NAC DTM are displayed (a). A DTM (5 m per pixel) created out of this LOLA data set is shown (b). Huge gaps between LOLA tracks (a) can be seen in the resulting DTM as homogeneously flat areas (b). A black rectangle indicates the size and location of the NAC DTM.

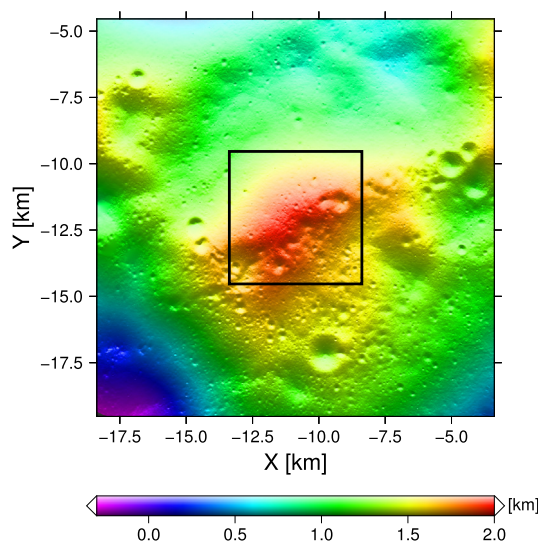


Fig. 6. (a) The final DTM_EV1 after co-registering all LOLA tracks intersecting the extended area. A black rectangle indicates the size and location of the NAC DTM.

area was chosen manually in a way that gaps between diverging tracks can still be interpolated reasonably (Fig. 5). Although, some small parts in the DTM are rather flat, the co-registration is still successful as seen in the fitting statistics and the quality of the final product (Fig. 6).

The DTM displayed in Fig. 5b is now co-registered to all LOLA tracks intersecting the extended area. The resulting DTM, referred to as DTM_EV1 (extended version 1), is shown in Fig. 6. Note, that areas formerly interpolated as flat surfaces are now filled with data from intersecting LOLA tracks (compare Figs. 5b and 6). DTM_EV1 serves now as the new base DTM and the previous step is repeated several times. The final extended version is displayed above in Fig. 1b.

3. Method

The purpose of the analysis is to derive illumination maps of polar landing sites at any given time to establish which sites are best suited for landers. Treating the Sun as a disk rather than a point source, each pixel value in an illumination map represents the fraction of the visible solar disk. By stacking illumination maps

over many time steps, various thematic maps can be computed, describing the duration and intensity of illumination for each pixel.

While Margot et al. (1999), Noda et al. (2008), Bussey et al. (2010) and McGovern et al. (2012) used ray-tracing methods to derive the illumination conditions at a given time, Mazarico et al. (2011) found advantages by using the so-called horizon method, which becomes especially efficient when looking at the same site over longer time scales involving many time steps. In the horizon method approach, the maximum angular elevation as seen from each pixel in a given azimuthal direction is calculated. For each azimuth direction one horizon map is stored, containing that maximum elevation value for each pixel (see Mazarico et al. (2011) for details). In this work the horizon method was used because long time scales are of interest.

The steps of deriving a simulated illumination for a certain region at a certain time are as follows:

1. This step has to be done only once (very time consuming computation),
 - (a) First horizon maps of the DTM for different azimuths have to be created, which is the most time consuming part in the analysis. For more details, see Section 3.1.
 - (b) A slope map of the DTM is calculated using a plane fit over 3×3 pixel (60×60 m) arrays.
2. This step has to be done at every time step (rather fast computation),
 - (a) For each time step t and each pixel in the area of interest, the azimuth and elevation of the Sun is calculated using the DE421 ephemeris (Folkner et al., 2009) and SPICE routines (Acton, 1996).
 - (b) The elevation of the horizon is compared to the elevation of the Sun in order to calculate the percentage of the visible solar disk. If necessary, the elevation of the horizon is computed through interpolation in the horizon maps. For more details, see Section 3.1.
 - (c) By comparing the slope map (local normal vector) with the Sun vector the solar incidence angle can be calculated which is used for photo-realistic rendering of the scene.

3.1. Illumination analysis

We produced a LOLA gridded DTM extending 200 km (83.4°S) around the lunar south pole (Fig. 1b). Although the area investigated extends to a few tens of kilometers only, the visible horizon from a random point on the Moon can be as far away as ~200 km.

For computational convenience, we chose the gnomonic projection, in which straight lines correspond to great-circle arcs on a sphere (Snyder, 1987).

The horizon maps can therefore easily be created from lines originating at each pixel in the direction of the considered azimuth direction. The elevation is then calculated along the line of sight with the simple relation $\arctan(\Delta h/s)$. Thereby, Δh is the height difference of a pixel on the line of sight to the observer pixel and s is the distance between the two. Obviously, distances measured in the map need to be corrected for the map distortion (gnomonic projection does not conserve distances). Also, the height differences need to be corrected for the curvature of the sphere. By using Cartesian coordinates, elevation angles may be derived from the dot product between the position vector to the observer pixel and the vector from the observer to the horizon (Fig. 7).

In total we calculate 720 horizon maps from 0° to 360° in 0.5° steps. The step size of 0.5° was chosen, as the Sun seen from the lunar surface has an angular diameter of $\sim 0.53^\circ$. This ensures that at least one azimuth direction of the 720 horizon maps lies within the Sun's angular diameter.

Horizon maps for any azimuth angle can be derived by linear interpolation of two neighboring horizon maps.

From the two adjacent horizon maps we must compute the fraction of the visible solar disk. A line crossing the two elevation angles at their azimuthal direction is drawn and the fraction above this line, which is the visible fraction of the Sun, is calculated (Fig. 8). Although the visible Sun fraction is estimated assuming a local linear horizon, the introduced error is negligible (De Rosa et al., 2012).

To simulate available sunlight at the solar panel of a large rover or a stationary lander, we may introduce height of the observer above the ground, when creating the horizon map database. Although these height values in reality might be small values (e.g. 1–10 m) they can make a substantial difference in Sun visibility. The Mars Science Laboratory (MSL) rover 'Curiosity', for instance, is equipped with the Mastcam imaging system operating ~ 2 m above ground (Bell et al., 2012), which reveals that such artificial heights are already achievable.

For studies of illumination over time, we use time steps of 1 h, during which the Moon rotates $\sim 0.5^\circ$, which corresponds to the Sun's angular diameter and the chosen azimuthal angular grid size. Hence we ensure that no azimuth gaps occur where the Sun could be completely blocked or fully visible (Fig. 9). Accurate estimates

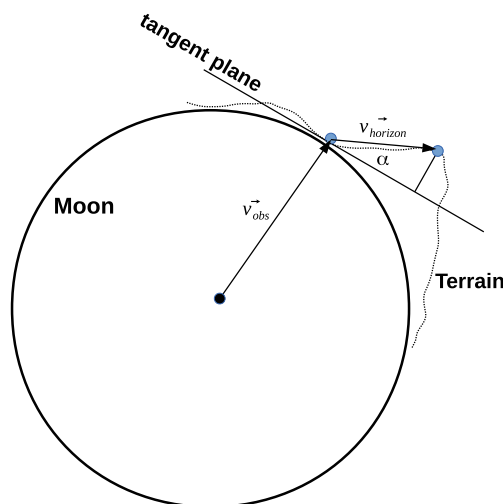


Fig. 7. Calculation of the elevation angle α as seen from a point on the lunar surface to the horizon.

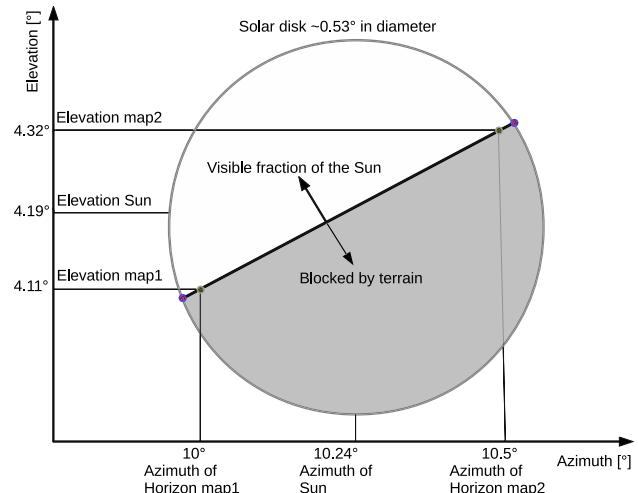


Fig. 8. Calculation of the fraction of the visible solar disk.

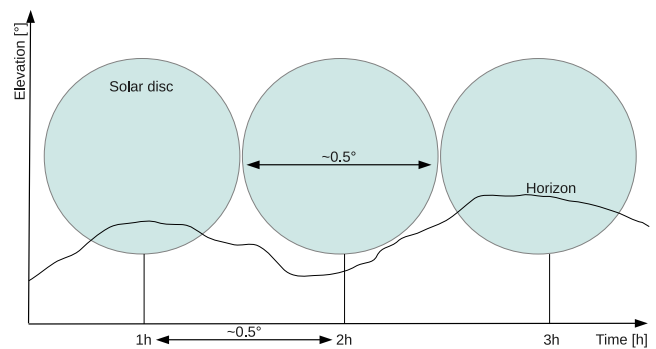


Fig. 9. This sketch shows an example where the Sun is completely visible at $t = 2$ h whereas it was partly blocked 1 h before and after ($t = 1$ h and $t = 3$ h).

for the visibility of the solar disk may be of practical interest as this will affect levels of sunlight in solar panels and power output. From illumination maps created for each time step we retrieve the temporal variations of illumination for each pixel in the area of interest, including knowledge about the beginning and the end of the illumination periods, see Fig. 18. Also, by stacking and averaging, illumination maps of the area can be created, where points of maximum and minimum illumination of interest for lunar landing can easily be found.

For comparisons with image data, we compute synthetic images. For simplicity, we adopt Lambertian shading, where surface brightness is proportional to the cosine of the incidence angle only (angle between the Sun vector and the surface normal vector). The computed surface brightness is then scaled by the fraction of the visible solar disk. For comparison, the NAC image is re-projected to match the geometry of the shaded DTM. This approach was used to render realistic scenes for validation purposes with NAC images (Section 4).

4. Validation of software and data

To validate the results from this investigation we compare the distribution of light and shadow in our synthetic images with selected NAC images (NAC image M139811097L/R for CR1 and M141385360L/R for SR1 and SR2). We selected NAC images showing the CR1 and SR1, SR2 landing sites. The synthetic images are computed for the imaged area and using the known time of image acquisition of these NAC images, see Fig. 10. Note, that the resolution difference between the NAC images and the simulated images

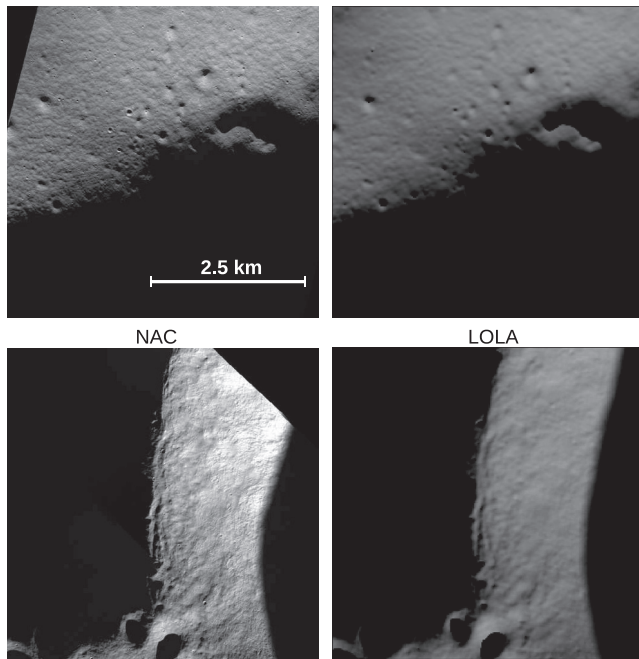


Fig. 10. Comparisons of NAC images and synthetic images computed from our LOLA DTM at NAC image acquisition time. Difference in brightness is due to surface variations in albedo which is not accounted for in the synthetic images. Note, that the synthetic images reproduce even small morphologic details. Left: NAC images of CR1 (M139811097L/R – upper image) and SR1, SR2 (M141385360L/R – lower image) potential landing site areas. Right: simulated illumination at CR1 (upper image) and SR1, SR2 (lower image) using LOLA data. The scale bar is valid for all images.

are of a factor 40 (0.5 m NAC image and 20 m LOLA synthetic image).

The comparison of simulated data with ground truth reveals that very small surface features of just a few pixels are reproduced in the simulation. Hence, accurate illumination information can be reproduced from the DTM.

5. Results

The analysis concentrates on three possible landing sites near the lunar south pole, two sites on Shackleton Rim (SR1 at 89.7742°S, 203.4952°E; SR2 at 89.6871°S, 197.0983°E) and one near “Connecting Ridge” (CR1 at 89.4555°S, 222.6192°E), which recently were also investigated by De Rosa et al. (2012) over a time period between October 22nd, 2018 – October 22nd, 2019. The illumination conditions were calculated for a 20 × 20 km region near the lunar south pole to generously cover the three landing sites. We choose time steps of 1 h resulting in 8,783 time steps (365 days and 23 h) when investigating the same period as De Rosa et al. (2012). Specifically, we compute the following quantities: accumulated illumination is the average of all visible fractions of the solar disk over the considered time period, e.g. if the Sun is always completely visible a percentage of 100% is assigned. Note that a random point on the lunar surface has an average illumination of 50% due to the diurnal cycle. However, a percentage of 50% does not necessarily imply that a certain area was in darkness for 50% of the considered time period, or that the area received constant sunlight from half of the solar disk. Further the sum of all times in darkness is calculated and referred to as accumulated percentage in darkness, e.g. if a location is 100 days in complete darkness over a considered period of 200 days a value of 50% is assigned. The accumulated percentage in sunlight is derived accordingly. The longest continuous time in darkness and the

longest continuous time in sunlight are also provided, e.g. a location can be in complete darkness for a total of 100 days as described above but the longest continuous period in complete darkness might only be 2.5 days.

5.1. Illumination conditions at the surface

We computed an accumulated illumination map of the south polar region at surface level (Fig. 11). We identify the 100 most illuminated areas, in which illumination levels range from 63.83% to about 73.70%. As is expected from previous studies (Bussey et al., 1999; Noda et al., 2008; Mazarico et al., 2011; De Rosa et al., 2012), CR1, SR1 and SR2 show illumination levels of 70% and more (Fig. 12). The three proposed stations in Speyerer and Robinson (2013) can also be found within the 100 most illuminated areas from this analysis. No areas of constant sunlight were found during the considered time period.

Several lines and clusters of above average illuminated small areas (>60%), further referred to as regions of interest (Rois), can be found along the ridge of the CR1 landing site (Fig. 12a). Despite the existence of several Rois, there is only an area of 400 m² (1 pixel) with an average illumination over 70% within the CR1 landing site.

The elongated SR1 area along the Shackleton Rim offers very good lighting conditions (Fig. 12b). An area of 1,200 m² (3 pixels) with illumination levels of more than 70% can be found, also containing the spot with the highest illumination (73.70%) in the study region (see Figs. 11 and 12b). Although the width of the Rois is very small, typically only 20 m (1 pixel), SR1 is an interesting landing site due to the quite large areal elongation of the Rois of up to 3,200 m² (~8 contiguous pixels), but also owing to the fact that the permanently shadowed Shackleton crater interior is right next to it (Mazarico et al., 2011; Bussey et al., 2010). Likewise, the

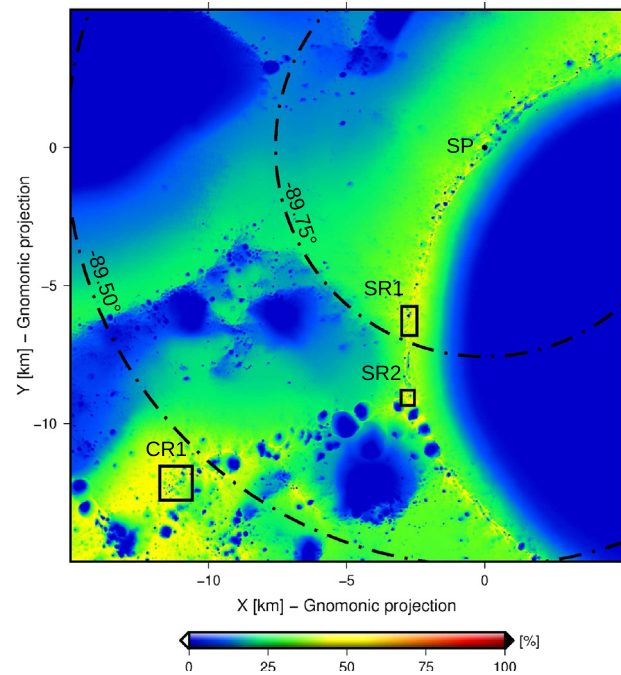


Fig. 11. Accumulated illumination map at the surface level ($h = 0$ m) from October 22nd, 2018 until October 22nd, 2019. The 3 landing sites CR1, SR1 and SR2 are bordered by a black box. The south pole (SP) and two parallels are also highlighted. The color bar indicates accumulated illumination over the considered time period. (For interpretation of the references to color in this figure legend, the reader is referred to the web version of this article.)

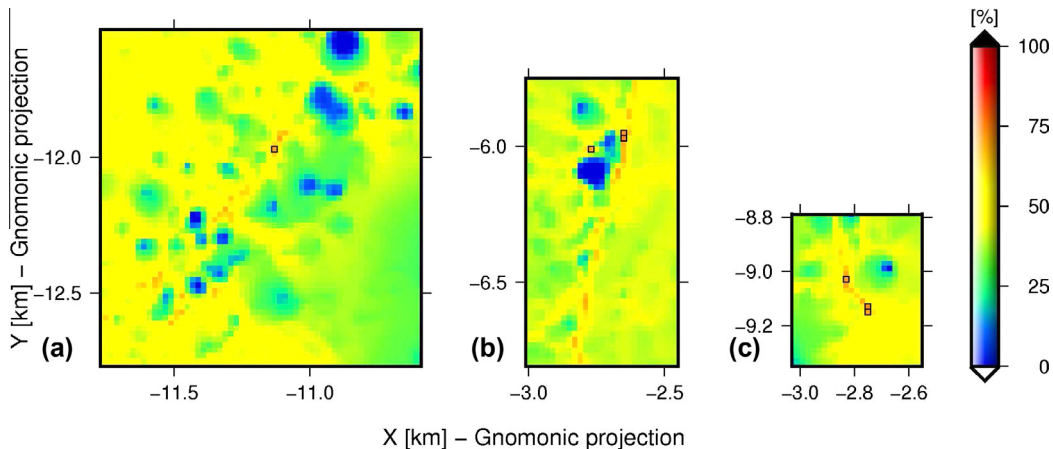


Fig. 12. Accumulated illumination at surface level. Reddish colors indicate RoIs with outlined pixels representing spots with an average illumination higher than 70%. (a): CR1 landing site area (89.4555°S , 222.6192°E). (b): SR1 landing site area (89.7742°S , 203.4952°E). (c): SR2 landing site area (89.6871°S , 197.0983°E). The color bar indicates accumulated illumination over the considered time period. (For interpretation of the references to color in this figure legend, the reader is referred to the web version of this article.)

elongated shape of SR2 contains an area of $1,200\text{ m}^2$ (3 pixels) with an illumination of more than 70%, similar to SR1 (Fig. 12c).

5.2. Illumination conditions at an altitude of 2 m

We also evaluated the illumination conditions for an observer elevated by 2 m, simulating the position of a solar panel on a stationary lander. Here, the accumulated map (Fig. 13) reveals substantially higher illumination levels. The areas of high illumination grow significantly and some of them become merged, compare Figs. 14 and 12. Contrary to the accumulated map at surface level (Fig. 11), the top most illuminated pixels are exclusively

found at the 3 landing sites SR1, SR2 and CR1 with an average illumination of $80.62\text{--}86.62\%$. The majority of those pixels (79 pixels) are found at CR1, revealing that this area benefits the most with an elevated solar panel (2 m above ground).

In total, an area of $\sim 120,000\text{ m}^2$ (297 pixels) receives more than 70% of average illumination at the CR1 landing site, see outlined pixels in Fig. 14a. The pixel with the highest illumination of 86.62% is also found here.

At SR1, a total area of $\sim 70,000\text{ m}^2$ (173 pixels), which is mainly continuous, shows an average illumination of more than 70%, see Fig. 14b. SR2 has an area of $\sim 12,000\text{ m}^2$ (49 pixels) with an average illumination of more than 70% which is completely continuous and is curve shaped, see Fig. 14c.

5.3. Illumination conditions at CR1 – long-term investigations

CR1 clearly stands out from the investigated landing sites with its comparably long illumination periods for a relatively large area (Fig. 14a). However, the orientation of the lunar rotation axis in inertial space varies with the precessional cycle of 18.6 years (Fig. 15). During this cycle certain polar areas could receive high illumination levels for several years but be darker on average at other times. To address the long-term stability of illumination levels at CR1, illumination over a time period covering the whole precessional cycle of 18.6 years is evaluated. Illumination levels over a period of 19 years, December 24, 2015 to December 24, 2034, are shown for observers at 0 m, 2 m and 10 m above surface level (see Figs. 16, 17 and 20).

Where only one pixel of high illumination exists regarding a time period of 1 year at surface level (Fig. 12a), 4 pixels are highly illuminated regarding the 19-year analysis (Fig. 16). The same analysis at 2 m height above the surface level (Fig. 17), leads to a similar result compared to the results in Fig. 14a for the 1-year analysis. An increase from 297 to 358 pixels with high illumination can be observed. The highest accumulated illumination is 88.12% and occurs at 89.4395°S , 222.8066°E (referred to as spot 1, Fig. 17), where the longest continuous period in darkness is 4.58 days and the longest continuous period in light is 233.87 days. The accumulated percentage in darkness and in light over the considered period is 8.00% and 92.00%, respectively. However, the smallest accumulated percentage in darkness is 7.73% and occurs at 89.4399°S , 222.8524°E (referred to as spot 2, Fig. 17). Consequently, spot 2 also has the highest accumulated percentage in light, which amounts to 92.27%. The longest continuous period in

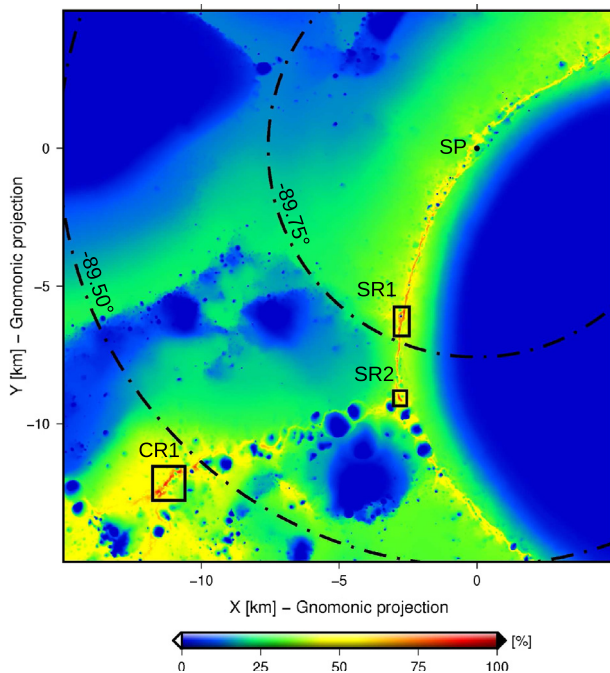


Fig. 13. Accumulated illumination map at 2 m above the surface level from October 22nd, 2018 until October 22nd, 2019. The 3 landing sites CR1, SR1 and SR2 are bordered by a black box. The south pole (SP) and two parallels are also highlighted. The color bar indicates accumulated illumination over the considered time period. (For interpretation of the references to color in this figure legend, the reader is referred to the web version of this article.)

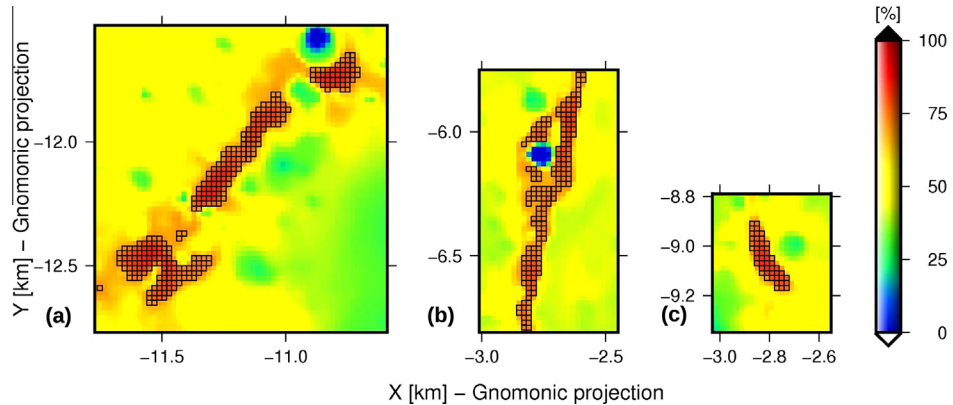


Fig. 14. Accumulated illumination 2 m above surface level. Reddish colors indicate Rols with outlined pixels representing spots with an average illumination higher than 70%. (a): CR1 landing site area (89.4555°S , 222.6192°E). (b): SR1 landing site area (89.7742°S , 203.4952°E). (c): SR2 landing site area (89.6871°S , 197.0983°E). The color bar indicates accumulated illumination over the considered time period. (For interpretation of the references to color in this figure legend, the reader is referred to the web version of this article.)

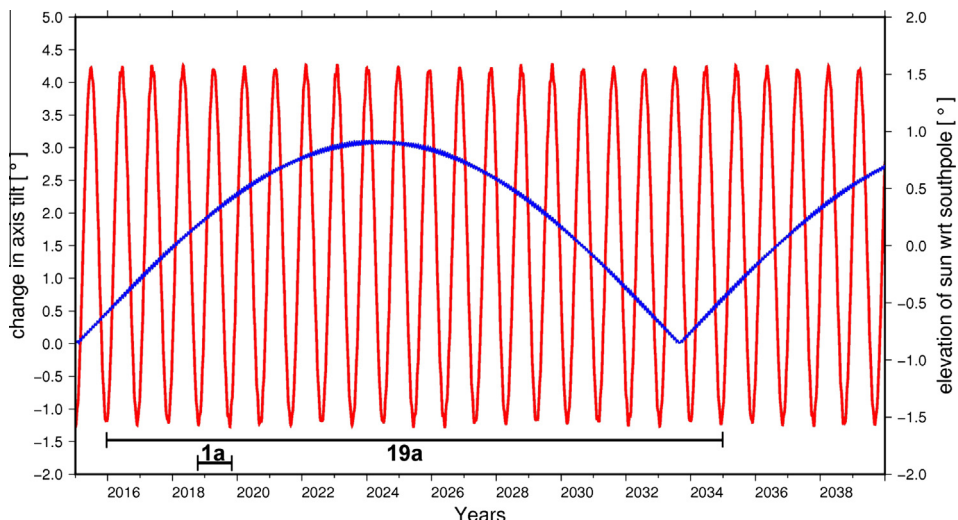


Fig. 15. The elevation of the Sun as seen from an observer at the lunar south pole is shown (red curve, right scale). Negative values indicate southern winter since the Sun is below the horizon. The precessional cycle (blue curve, left scale) is shown as the change in axis tilt with respect to the axis tilt in 2015. The short horizontal bar shows the 1-year time period evaluated for the three landing sites, whereas the long bar indicates the 19-year evaluation done for CR1. (For interpretation of the references to color in this figure legend, the reader is referred to the web version of this article.)

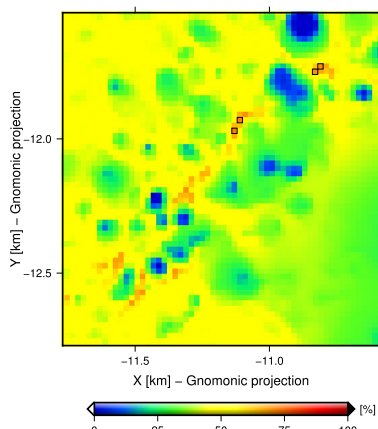


Fig. 16. Accumulated illumination map of CR1 (89.4555°S , 222.6192°E) over a period of 19 years at surface level. Outlined pixels represent spots with an average illumination higher than 70%. The color bar indicates accumulated illumination over the considered time period.

darkness and light at that location is 4.62 days and 233.87 days, respectively, with an accumulated illumination of 87.93%. Spot 1 and spot 2 are located right next to each other and are almost identical in their illumination properties. A plot of illumination versus time as well as a horizon plot for spot 1 are shown in Figs. 18 and 19. It can be noted, that even at lunar southern winter when the Sun is lowest over the horizon, illumination levels are still substantial.

We also computed the accumulated illumination for an observer 10 m above ground (Fig. 20). In total 1,724 pixels ($\sim 0.7 \text{ km}^2$) are now highly illuminated. The location of highest illumination, 92.55%, is located at 89.4516°S , 222.7581°E (referred to as spot 3, Fig. 20). The accumulated percentage in darkness is 4.39% and consequently 95.61% in light, with the longest continuous periods in darkness and light being 3.08 days and 262.42 days, respectively. The longest accumulated period in light and therefore shortest period in darkness is found at location 89.4544°S , 222.8445°E and amounts to 4.35% for the dark period and 95.65% for the illuminated period (referred to as spot 4, Fig. 20). The average illumination is 91.94% with the longest continuous period of darkness being 3.17 days and the longest continuous period in light being

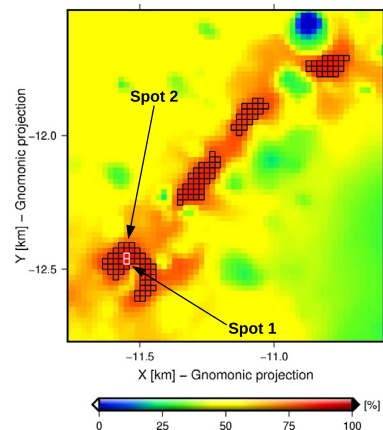


Fig. 17. Accumulated illumination map of CR1 (89.4555°S , 222.6192°E) over a period of 19 years at 2 m height above the surface level. Black outlined pixels represent spots with an average illumination higher than 80%. Spots 1 and 2 are outlined in white. The color bar indicates accumulated illumination over the considered time period. (For interpretation of the references to color in this figure legend, the reader is referred to the web version of this article.)

262.42 days. Spot 3 and spot 4 are located 90 m from each other and are almost identical in their illumination levels. A plot of illumination versus time and a horizon plot for spot 3 are shown in Figs. 21 and 22.

A list of the highest illumination spots found in previous studies is shown in Table 1, see also Speyerer and Robinson (2013). Results from different studies can only be compared when evaluated over the same time period for reasons of planetary constellation and the influence of the lunar precessional cycle. We compare our long-term study of 19 years with that carried out by Mazarico et al. (2011) for observers at 0 m and 10 m above ground. An additional 6-months analysis (March 31, 2010 to September 24, 2010) was carried out to compare our results from surface levels with De Rosa et al. (2012).

In an analysis evaluated at surface level and over a 6-months period, De Rosa et al. (2012) found the location receiving the most illumination within the SR2 landing site area. In this study, however, we find the location receiving the most illumination within the SR1 landing site area (compare points 4 and 6 in Fig. 24 and Table 1). The finding of different locations in the two studies can be explained by the different resolutions of the used LOLA DTMs. For instance, when we reduce the original resolution of our 20 m/pixel LOLA DTM to 40 m/pixel as used in De Rosa et al.

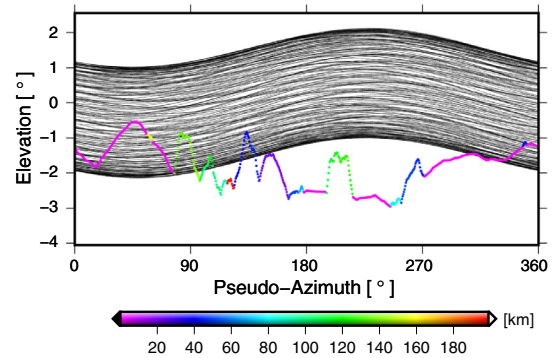


Fig. 19. Plot of the horizon as seen from spot 1 at 2 m above surface level. The horizon line is color-coded by the distance to the obstructing topography (horizon). The black lines show the trajectory of the center of the Sun as seen from spot 1 over the 19-year period. Spot 1 is located at 89.4395°S , 222.8066°E . (For interpretation of the references to color in this figure legend, the reader is referred to the web version of this article.)

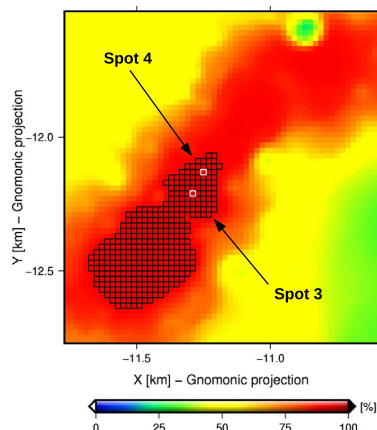


Fig. 20. Accumulated illumination map of CR1 (89.4555°S , 222.6192°E) over a period of 19 years at 10 m height above the surface level. Black outlined pixels represent spots with an average illumination higher than 92%. Spot 3 and 4 are outlined in white. The color bar indicates accumulated illumination over the considered time period. (For interpretation of the references to color in this figure legend, the reader is referred to the web version of this article.)

(2012), we can reproduce their results (compare points 4 and 5 in Fig. 24 and Table 1).

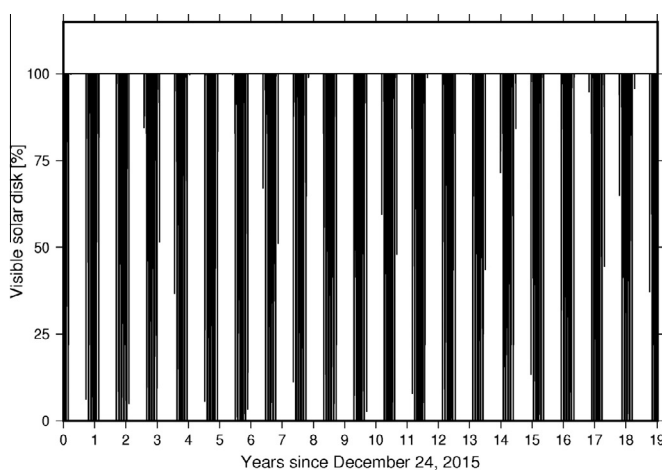
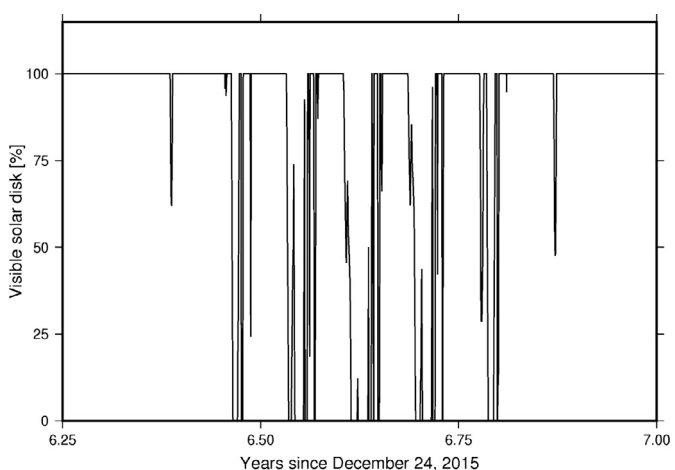


Fig. 18. Plot of visible solar disk versus time for spot 1 at 2 m above surface level. Between periods of constant illumination, periods of rapidly changing lighting conditions occur (see zoom in at right hand plot). These times coincide with lunar southern winter. Spot 1 is located at 89.4395°S , 222.8066°E .



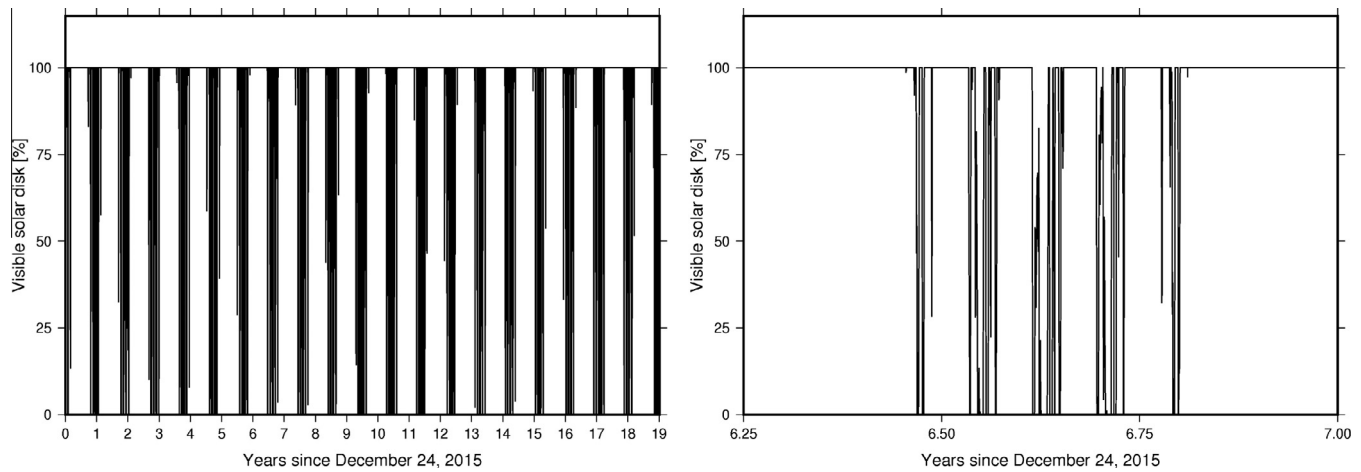


Fig. 21. Plot of visible solar disk versus time for spot 3 at 10 m above surface level. Between periods of constant illumination, periods of rapidly changing lighting conditions occur (see zoom in at right hand plot). These times coincide with lunar southern winter. Spot 3 is located at 89.4516°S, 222.7581°E.

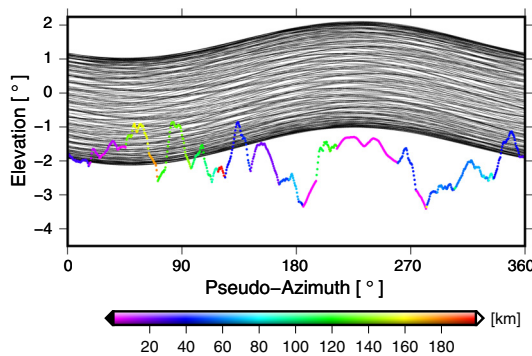


Fig. 22. Plot of the horizon as seen from spot 3 at 10 m above surface level. The horizon line is color-coded by the distance to the obstructing topography (horizon). The black lines show the trajectory of the center of the Sun as seen from spot 3 over the 19 years period. Spot 3 is located at 89.4516°S, 222.7581°E. (For interpretation of the references to color in this figure legend, the reader is referred to the web version of this article.)

Similar to the previous comparison, Mazarico et al. (2011) identified the maximum illuminated spot in their long-term analysis

evaluated at surface level at the CR1 landing site, whereas this study finds the maximum spot at SR2 when running simulations over the 19-year period (compare points 7 and 9 in Fig. 24 and Table 1). The results can be reproduced, however, when we reduce the resolution to 240 m/pixel as used in their study (compare points 7 and 8 in Fig. 24 and Table 1). Note, that the location receiving maximum illumination in the 19-year study at surface level in this work is almost identical with the location found by De Rosa et al. (2012) and station 1 (89.685°S, 196.7°E) identified by Speyerer and Robinson (2013) in their 1-year period study (compare points 4 and 9 in Fig. 24 and Table 1).

The spot of maximum illumination found by Mazarico et al. (2011) simulated 10 m above ground is located 52 m away from the one found in this work, corresponding to only 1/5th of the pixel resolution used in their study (240 m). Hence, the found locations can be considered identical even though vastly different resolutions were used (compare points 12 and 13 in Fig. 24 and Table 1).

The differences in the three studies at surface level can be explained by the dependency of the analysis on raw data density, the local topography and, therefore, the interpolation algorithms that are used. At surface level, topography in the near-field is dominating the amount of received illumination and resolution

Table 1

List of points with highest illumination at the lunar south polar region of previous studies in combination with several points found in this study. The last column shows the evaluated period, where studies over the full lunar precessional cycle are marked “lpc”. All results retrieved in this work that can be compared to previous studies are highlighted.

P.	Study	Res. (m/pix)	III. (%)	Location latitude, longitude	h (m)	Period (a)	Site
1	Noda et al. (2008)	474	86	-88.8, 124.1	0	lpc	–
2	Bussey et al. (2010)	474	86	-88.74, 124.5	0	lpc	–
3	Speyerer and Robinson (2013)	100	71.7	-89.74, 201.20	0	1.0	–
4	De Rosa et al. (2012) ^a	40	84.13	-89.687, 196.144	0	0.5	SR2
5	This study ^a	40	81.30	-89.6871, 197.2887	0	0.5	SR2
6	This study ^a	20	73.84	-89.7846, 203.9358	0	0.5	SR1
7	Mazarico et al. (2011)	240	89.01	-89.45, 222.69	0	lpc	CR1
8	This study	240	86.84	-89.44, 222.52	0	lpc	CR1
9	This study	20	76.23	-89.6856, 196.7626	0	lpc	SR2
10	This study (spot 1)	20	88.12	-89.4395, 222.8066	2	lpc	CR1
11	This study (spot 2)	20	87.93	-89.4399, 222.8524	2	lpc	CR1
12	Mazarico et al. (2011)	240	93.10	-89.45, 222.69	10	lpc	CR1
13	This study (spot 3)	20	92.55	-89.4516, 222.7581	10	lpc	CR1
14	This study (spot 4)	20	91.94	-89.4544, 222.8445	10	lpc	CR1

^a The period evaluated was 6 months, March 31, 2010 – September 24, 2010.

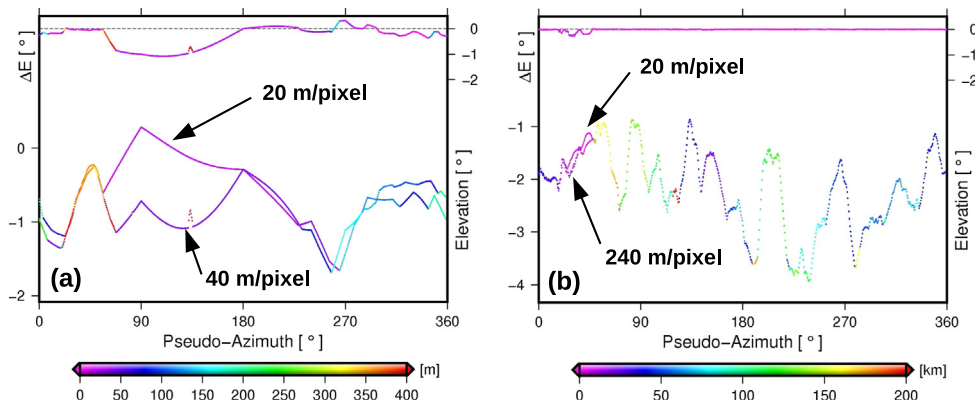


Fig. 23. Horizons and differences between horizons are color coded by distance. (a) Comparison of the local horizon of spot 1 derived from a 20 m/pixel and 40 m/pixel DTM at surface level (distance scale in meter). It can be noted, that the horizon calculated from the 20 m/pixel DTM generally is higher in the near-field than the horizon from the 40 m/pixel DTM. (b) Comparison of the local horizon of spot 1 derived from a 20 m/pixel and 240 m/pixel DTM at 10 m above ground (distance scale in kilometer). In the far-field the two horizons are identical and only small differences appear in the rather short portion of the near-field, where the horizon of the 20 m/pixel lies above the horizon of the 240 m/pixel DTM. (For interpretation of the references to color in this figure legend, the reader is referred to the web version of this article.)

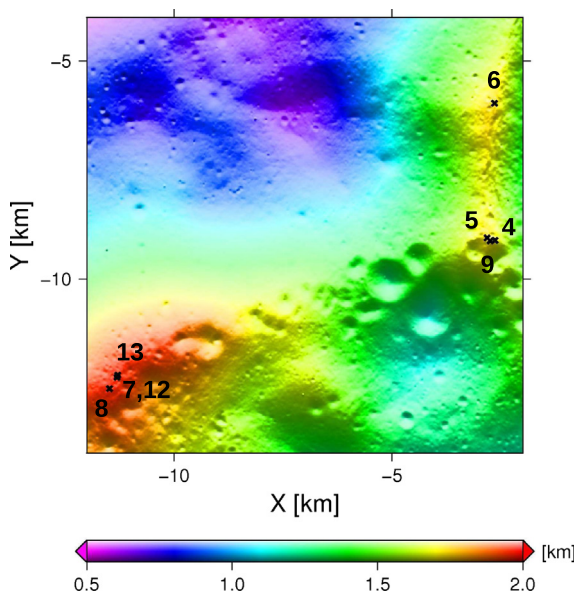


Fig. 24. Overview of spots of maximum illumination found in different studies. Point numbers correspond to the first column in Table 1.

differences will have a great influence on the result (compare points 4, 6 and 7, 9 in Table 1). A plot of the local horizon of the same viewing point derived from a 20 m/pixel and a 40 m/pixel DTM is shown in Fig. 23a. Here, the significance of local topography can be seen, where a higher resolved horizon is generally above the lower resolved horizon, which results in lower illumination levels. The far distant topography is of greater interest for simulations carried out higher above surface level, e.g. 10 m above ground, where most of the near-field can be looked across. Here, the resolution of the DTM is of minor significance, compare points 12, 13 in Table 1 and Fig. 23b. In general, small height differences in corresponding DTM pixels can occur when using different resolutions, different interpolation methods or different LOLA spots and will have a great impact on the elevation angles calculated in the near-field but are negligible when calculating elevation angles in the far-field.

An overview of the distribution of points with maximum illumination retrieved by Mazarico et al. (2011), De Rosa et al. (2012) and this study, is shown in Fig. 24.

5.4. Surface slopes

Surface slopes are a critical parameter for safe landing and must be taken into account for site selection (e.g., Golombek et al., 2003). In this work only areas with moderate slopes less than 5° are

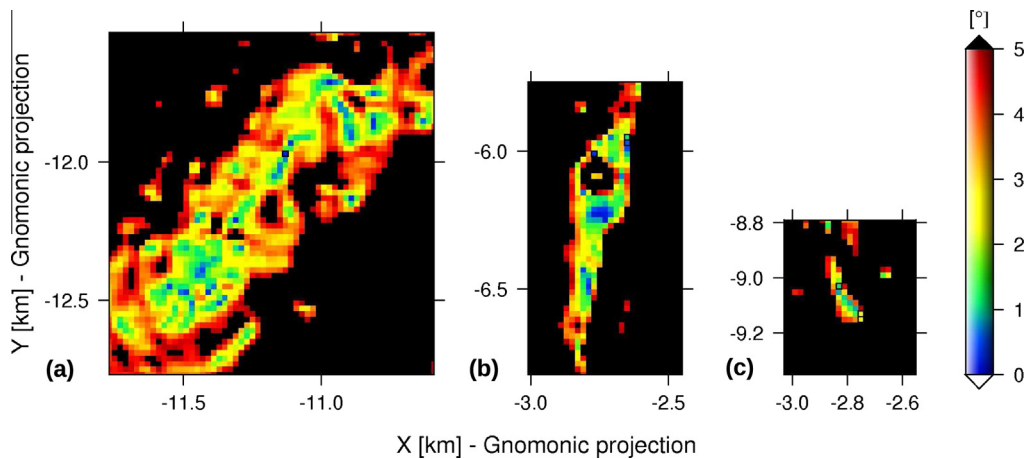


Fig. 25. Slope maps of the CR1, SR1 and SR2 landing site. Only slopes of $<5^\circ$ are color coded, steeper slopes are considered too hazardous for landing or roving. (For interpretation of the references to color in this figure legend, the reader is referred to the web version of this article.)

considered possible landing sites although some landers are designed to manage slopes of up to 15° (De Rosa et al., 2012). Most surface slopes at the CR1 and SR1 are smaller than 3° (Figs. 25a and b). SR2 has slightly steeper slopes in some parts, but for most of the area, landing is possible on terrain with slopes smaller than ~3–4° (Fig. 25c). At surface level, the dimensions of potential landing sites are comparable in both maps, the slope and the illumination map (Figs. 12 and 25). At 2 m above ground, however, the SR2 landing site (Fig. 14c) proves to be more limited by rough terrain than by illumination. The RoI of illumination at CR1 (Fig. 14a) is still surrounded by a zone of slopes of <5° whereas SR1 now more or less covers the whole 5° slope map (Fig. 14b). Only at 10 m above ground the RoI of illumination at CR1 fills the entire 5° slope map and beyond (see Fig. 20).

In Fig. 26 the accumulated illumination of each pixel at CR1, SR1 and SR2 at 0 m, 2 m and 10 m above ground is plotted against the

surface slope at that particular location. The amount of data points is proportional to the considered area. All data points that exhibit accumulated illumination beyond 70% at slopes less than 5° are plotted in red. As expected, the amount of points satisfying these constraints grows when we elevate our observer from 0 m to 2 m and further to 10 m above ground. However, at SR1 and SR2 distinct horizontal lines occur at 10 m above ground. This indicates, that a level of saturation is reached somewhere between 2 m and 10 m where further elevating does not have an immediate effect on the maximum accumulated illumination. This can be explained by the fact that all data points on these lines now see the same horizon and most of the near field is overlooked. If we elevated the observer further the final stage would be a single line at 100% accumulated illumination, a point of eternal light, which might be kilometer away from the lunar surface. In between, these lines will move more or less as a whole due to the almost identical

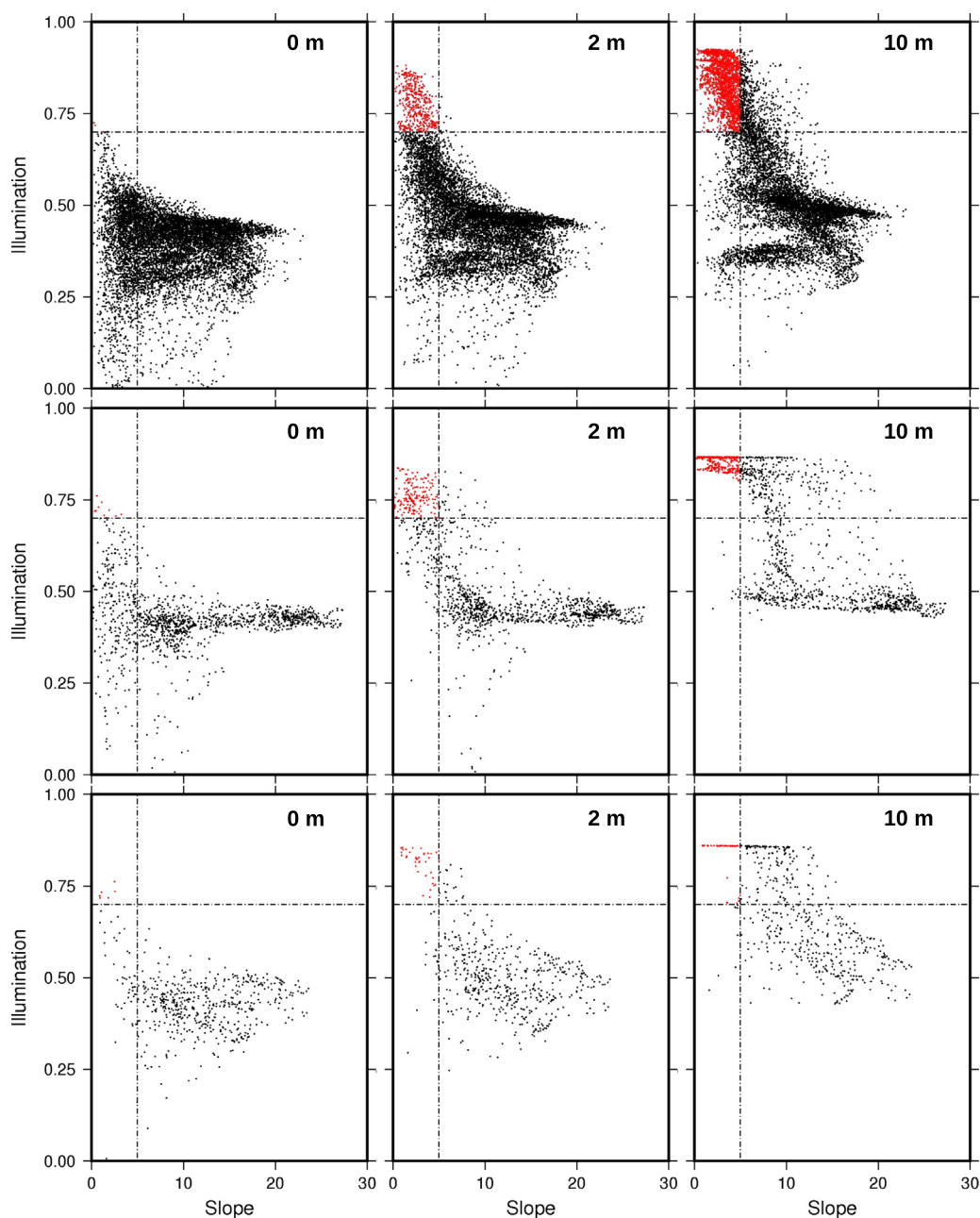


Fig. 26. Slopes vs. accumulated illumination at CR1, SR1 and SR2 landing site (top-bottom) at surface level, 2 m and 10 m above ground (left-right). Locations with slopes <5° and illumination >70% (RoI), are more frequent the higher the elevation above ground.

horizons. Only at CR1 no distinct intermediate saturation level is reached due to the larger extent of the area resulting in many independent horizons. Elevating the observer further, however, would lead to converging of data points to more distinct lines.

6. Conclusion

We simulated illumination conditions at the lunar south pole and investigated three sites in detail, the “Connecting Ridge” (CR1) between the Shackleton and de Gerlache crater and two locations on the Shackleton Rim (SR1, SR2). This work revealed that CR1 benefits the most (~80% of the highest illuminated pixels are found here, see Section 5.2) in received illumination when elevating a solar panel 2 m above ground. We therefore conclude that for a robotic mission relying on solar power collected by panels above surface level, CR1 is probably the most promising location at the lunar south pole. The locations we find for maximum illumination at surface level differ from those found by Mazarico et al. (2011) and De Rosa et al. (2012). However, when elevating a solar panel 10 m above ground the location found in this work is within the pixel found by Mazarico et al. (2011). This is a strong indicator, that near-surface illumination predictions are highly dependent on the local topography and on the interpolation algorithms being used. Hence, DTMs of high accuracy and resolution are needed for investigations on illumination conditions at possible landing sites.

Acknowledgments

P. Gläser was funded by a Grant of the German Research Foundation (FOR 1503, OB 124/8-1). Parts of this work were also supported by a Grant of the German Space Agency (FKZ 50OW1202). We wish to thank the LOLA and LROC Science Team for releasing such great data products.

References

- Acton, C.H., 1996. Ancillary data services of NASA's navigation and ancillary information facility. *Planet. Space Sci.* 44, 65–70.
- Bell, J.F., et al., 2012. Mastcam multispectral imaging on the Mars science laboratory rover: Wavelength coverage and imaging strategies at the gale crater field site. *Lunar Planet. Sci.*, p. 2541.
- Bussey, D.B.J., McGovern, J.A., Spudis, P.D., Neish, C.D., Noda, H., Ishihara, Y., Sørensen, S.A., 2010. Illumination conditions of the south pole of the Moon derived using Kaguya topography. *Icarus* 208, 558–564.
- Bussey, D.B.J., Spudis, P.D., Robinson, M.S., 1999. Illumination conditions at the lunar south pole. *Geophys. Res. Lett.* 26, 1187–1190.
- Carpenter, J.D., Fisackerly, R., De Rosa, D., Houdou, B., 2012. Scientific preparations for lunar exploration with the European lunar lander. *Planet. Space Sci.* 74, 208–223, 1207.4965.
- Chakraborty, S., 2011. The Co-alignment of Planetary Laser Altimeters and their Use for Surface Roughness Investigations. University of Bern, PhD-Thesis, 182.
- Chin, G. et al., 2007. Lunar reconnaissance orbiter overview: The instrument suite and mission. *Space Sci. Rev.* 129, 391–419.
- De Rosa, D. et al., 2012. Characterisation of potential landing sites for the European space agency's lunar Lander project. *Planet. Space Sci.* 74, 224–246, 1208.5587.
- Folkner, W.M., Williams, J.G., Boggs, D.H., 2009. The Planetary and Lunar Ephemeris DE 421. *Interplanetary Network Progress Report* 178, C1.
- Gläser, P., Haase, I., Oberst, J., Neumann, G.A., 2013a. Co-registration of laser altimeter tracks with Digital Terrain Models and applications in planetary science. *Planet. Space Sci.* 89, 111–117.
- Gläser, P., et al., 2013b. Improvement of local LOLA DTMs using LROC NAC DTMs – Example for an ESA lunar Lander candidate landing site. *Lunar Planet. Sci. Abstract* 1967, p. 1719.
- Golombek, M.P. et al., 2003. Selection of the Mars exploration rover landing sites. *J. Geophys. Res. (Planets)* 108, 8072.
- Margot, J.L., Campbell, D.B., Jurgens, R.F., Slade, M.A., 1999. Topography of the Lunar poles from radar interferometry: A survey of cold trap locations. *Science* 284, 1658–1660.
- Mazarico, E., Neumann, G.A., Smith, D.E., Zuber, M.T., Torrence, M.H., 2011. Illumination conditions of the lunar polar regions using LOLA topography. *Icarus* 211, 1066–1081.
- McGovern, J.A., et al., 2012. Mapping and characterization of non-polar permanent shadows on the lunar surface. *Lunar Planet. Sci.*, p. 2550.
- Neumann, G., 2009. Lunar Orbiter Laser Altimeter Raw Data Set, LRO-L-LOLA-3-RDR-V1.0, NASA Planetary Data System.
- Noda, H. et al., 2008. Illumination conditions at the lunar polar regions by KAGUYA(SELENE) laser altimeter. *Geophys. Res. Lett.* 35, 24203.
- Robinson, M.S. et al., 2010. Lunar Reconnaissance Orbiter Camera (LROC) instrument overview. *Space Sci. Rev.* 150, 81–124.
- Shoemaker, E.M., Robinson, M.S., Eliason, E.M., 1994. The south pole region of the Moon as seen by Clementine. *Science* 266, 1851–1854.
- Smith, D.E. et al., 2010a. The Lunar Orbiter Laser Altimeter investigation on the Lunar Reconnaissance Orbiter Mission. *Space Sci. Rev.* 150, 209–241.
- Smith, D.E. et al., 2010b. Initial observations from the Lunar Orbiter Laser Altimeter (LOLA). *Geophys. Res. Lett.* 371, 18204.
- Snyder, J.P., 1987. Map Projections: A Working Manual. Geological Survey (U.S.).
- Speyerer, E.J., Robinson, M.S., 2013. Persistently illuminated regions at the lunar poles: Ideal sites for future exploration. *Icarus* 222, 122–136.
- Stacy, N.J.S., Campbell, D.B., Ford, P.G., 1997. Arecibo radar mapping of the lunar poles: A search for ice deposits. *Science* 276, 1527–1530.
- Watson, K., Murray, B., Brown, H., 1961. On the possible presence of ice on the Moon. *J. Geophys. Res.* 66, 1598–1600.